Laser 3D printing of complex copper structures

Loïc Constantin, Zhipeng Wu, Nan Li, Lisha Fan, Jean-François Silvain, Yong Feng Lu

Laser 3D printing of Complex Copper Structures

Loic Constantin,[1,2,‡] Zhipeng Wu,[1,‡] Nan Li,[1] Lisha Fan,[1,] Jean-Francois Silvain[1,2,*] and, Yong Feng Lu,[1,*]*

[1] Department of Electrical and Computer Engineering, University of Nebraska-Lincoln, Lincoln, NE, 68588.

[2] CNRS, Univ. Bordeaux, Bordeaux INP, ICMCB, UMR 5026 F-33608 Pessac, France.

Keywords: additive manufacturing, copper, selective laser melting, thermal management, heat sinks

ABSTRACT: The ability to design complex copper (Cu) parts into the most efficient thermal structures is an old dream, but difficult to realize with conventional manufacturing techniques. The recent development of laser 3D printing techniques makes it possible to fully explore intricate designs and maximize the thermal performance of Cu-based thermal management components but present significant challenges due to its high optical reflectivity. In this study, we demonstrated the laser 3D printing of pure Cu with a moderate laser power (400 W). Dense Cu parts (95 %) with smooth surface finishing (R_a ~18 μm) were obtained at a scan speed of 400 mm/s, a hatch distance of 0.12 mm, and a layer thickness of 0.03 mm. The hardness, electrical, and thermal conductivity of the printed Cu parts are 108 MPa, 5.71×10^7 S/m, and 368 W/m·K, respectively, which are close to those of bulk Cu. Additionally, complex heat sink structures were printed with large surface areas (600 mm^2/g), and their cooling performances were compared to a commercial heat sink with a smaller surface area (286 mm^2/g) on an electronic chip. The complex heat sinks printed cools the electronic chip 45% more efficiently than the commercial one. The introduction of selective laser melting to additively manufacturing Cu heat

sinks offers the promise to enhance the performance beyond the scope of exciting thermal management components.

INTRODUCTION

The high thermal conductivity (~ 400 W/m·K) of pure copper (Cu) makes it an essential material for thermal management applications in numerous industries, such as microelectronic manufacturing, power plants, and aerospace[1–5]. However, the shape (*i.e.*, surface area) of heat sinks plays a crucial role in heat dissipation, and due to the current fabrication limitation is often a simple geometry [6,7]. Recently, the development of additive manufacturing, especially selective laser melting (SLM), has attracted tremendous attention due to its ability to efficiently manufacture complex geometrical metal parts while minimizing waste products and post-processing steps [7,8]. The thin and sophisticated features enabled by SLM and the excellent properties of bulk Cu have the potential to significantly enhance the efficiency of heat sinks components [9,10].

In the past, few attempts have been undertaken to additively manufacture pure Cu [11]. Silbernagel *et al.* and Jadlhav *et al.* studied the fabrication of Cu parts by SLM using low laser powers of 200 and 300 W, respectively [12,13]. Low-density parts (86%) with low thermal conductivity (TC) of 202 W/m·K were reported. The low-density parts resulted from insufficient laser energy deposited on powders due to the fast heat dissipation rate and the low laser absorption in the near-infrared (IR) domain of Cu [14,15]. High laser power (800 W) was employed to overcome this issue, and dense Cu parts were printed (97%) with a TC of 336 W/m·K [16,17]. Nevertheless, the high reflectivity of Cu can severely damage the laser optics, leading to high maintenance and operation costs [12]. Another approach is to print Cu alloys that

have much higher laser absorption rates than pure Cu. Serval studies reported the production of fully dense Cu-alloys such as Cu-Cr, Cu-Sn, or Cu-Zn[18–20]. However, a post-processing step is required on the as-built Cu alloys to reach an electrical and thermal properties close to bulk Cu [18,19]. Despite these impressive results, SLM of pure Cu with properties comparable to bulk Cu without post-processing remains challenging.

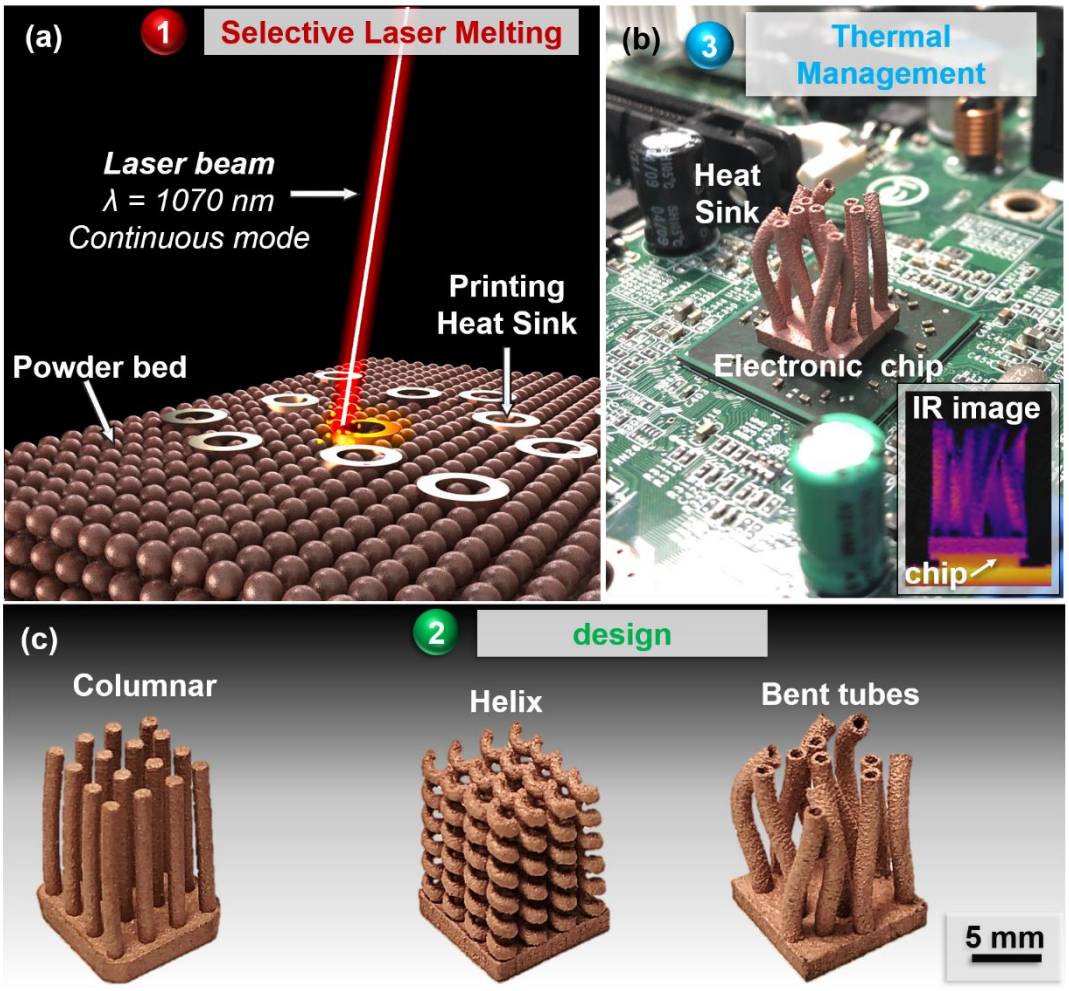

Figure 1. (a) Schematic illustration of the SLM process to print Cu heat sinks, **(b)** photo of a printed heat sink on an electronic chip with the thermal image in the insert, and **(c)** photos of three complex-shaped heat sink structures printed: columnar, helix, bent tubes

In this study, the advantage of SLM in the fabrication of heat sinks was demonstrated by additively manufacture passive heat sinks for electronic devices using a moderate laser power (400W) (**Figure 1 (a)**). Complex shaped, dense, and crack-free heat sinks were fabricated by SLM after optimizing the printing parameters (**Figure 1 (c)**). The heat dissipation performance of the heat sinks printed was compared to the commercial one (COM, Enzotech Mosfet MOS-C10) by studying the temperature profile of a hot electronic chip cooled by the heat sinks. (**Figure 1 (b)**). It is shown that the printed heat sink structures with high-surface-area printed outperform the COM one. SLM-based 3D printing technique offers an easy and effective method to designing complex geometric shapes, ultimately improving the thermal performance of heat sinks components.

EXPERIMENTAL SECTION

Cu parts were fabricated by SLM using an SLM 125 3D printer (SLM Solutions). The printing parameters are summarized in **Figure 2 (a)**. The printer is equipped with a continuous wave (CW) fiber laser (IPG photonics, YLM, Yb: YAG, λ = 1070 nm). The maximum output power is 400 W with a spot diameter of 70 μm on the powder bed surface. Spherical Cu powders with an average size of 45 μm were used in this study (US Nano, Cu 99.5%). A scanning electron microscopy (SEM) micrograph of the powders is presented in **Figure 2 (a)**. The printing chamber was filled with argon (Ar) (99.9%, Matheson) to reduce an oxygen level below 0.09%. A constant pressure of 18 mbar was maintained during all experiments. The printing parameters were optimized by adjusting the hatch distance from 0.08 to 0.12 mm, and the scan speed from 200 to 600 mm/s. The laser power and layer thickness were kept constant at 400 W and 0.03 mm, respectively, throughout the study. A stripe scan strategy was used in this study, as illustrated in **Figure 2 (c).** The structures printed were designed using SolidWork®. Magics®

software was used to prepare print jobs and establish the printing parameters. The parts were printed on a stainless-steel building plate (stainless steel, 123 × 123 × 25 mm^3).

(a) Parameters	Values
Spot Size	70 μm
Laser Power	400 W
Scan Speed	200 to 600 mm/s
Hatch Distance	0.08 to 0.12 mm
Layer thickness	30 μm
Powder size	45 μm

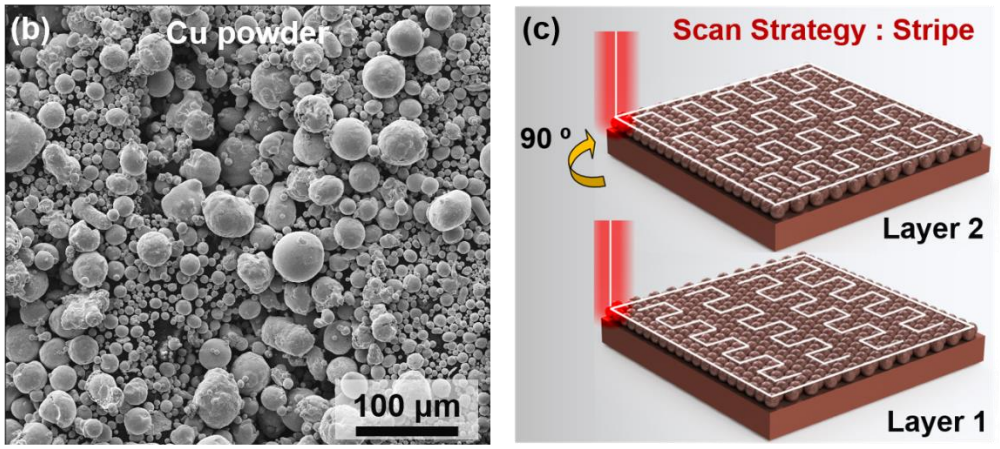

Figure 2. (a) SLM parameters used in this study, **(b)** SEM micrographs of the copper powder, and **(c)** schematic illustration of the stripe scan strategy.

The density of the samples was measured using the Archimedes method (Mettler Toledo AT201). The microstructure of the printed parts was characterized using a scanning electron microscope (SEM, FEI Quanta 200 Environmental SEM). The cross-sectional views of the polished samples were observed using an optical microscope (Nikon Eclipse E600). The average surface roughness was measured using an optical surface profiler (Zygo NewView 8000). The

crystalline phases of the powders and parts printed were analyzed by X-Ray diffraction (XRD, Bruker-AXS D8 Discover Diffractometer, Cu Kα = 0.154 nm). Energy dispersive X-Ray (EDX) was performed on the Cu powder and part using a Helios NanoLab™ 660 equipped with an EDAX™ detector. The electrical resistance of the printed material was measured using a four-point probe method (Keithley 2400 Source Meter) with a current ranging from -0.03 to 0.03 A. The thermal conductivity was calculated from the electrical conductivity using the Wiedemann-Franz law. Sample hardness was measured by Vickers hardness test (Wilson Tukon™ 2500-3), using a load and dwell time of 0.5 Kg and 10 s, respectively. The physical properties of the heat sinks printed were compared to a commercial Enzotech Mosfet MOS-C10 heat sink. The thermal-dissipation performances of the printed heat sinks were evaluated by simulating the thermal management situation of microelectronics using an IR camera (FLIR E85 24º). The heat sinks were attached to an electronic chip with a thermal tape (3M™ 8815 Thermal Tape). Using a hot plate, the memory card and the heat sink were heated to 100, 150, and 200 ºC, respectively, with a fan, which was placed 10 cm above the heat sink for airflow.

RESULTS AND DISCUSSION

Reports on the 3D laser printing of pure Cu show that high laser power is required to obtain dense Cu parts. The printing parameter windows typically reported are a laser power between 600 to 1000 W, a scan speed comprise between 200 to 1000 mm/s, a layer thickness between 0.03 to 0.05, and a hatch distance from 0.05 to 0.12 mm [12,16,17]. Thus, the printing parameters were optimized in the range of the same parameters as found in the literature to achieve dense Cu parts with smooth surface finishes but by using a moderate laser power of 400 W. The hatch distance was adjusted from 0.08 to 0.12 mm at an increment of 0.01 mm. The scan speed increased from 200 to 600 mm/s with a 50 mm/s increment. The layer thickness was kept

at fixed values of 0.03 mm. First, the overall shape of the printed parts was investigated and qualitatively categorized into three groups, which defined the process window of pure Cu. **Figure 3 (a)** and **(b)** show a photo of the printed parts on the base plate and a 2D map depicting the quality of the parts at different scan speeds and hatch distances—cracked, good, and porous samples are represented by green squares, red circles, and blue triangles, respectively. A low scan speed (200 to 350 mm/s) resulted in cracked samples for all the hatch distances studied. With a low scan speed, the energy deposited greatly exceeded the amount required to melt the Cu powders. The high temperature of the molten pool generated a large thermal gradient in the solid Cu, which ultimately caused interlayer delamination and debonding from the build plate [21–23]. Note that, at a scan speed of 200 mm/s (**Figure 3 (a)**), the print was stopped because bending/debonding of Cu from the build plate caused severe damage to the powder recoater. Printing with a higher scan speed of 400 mm/s and a hatch distance of 0.12 mm produced smooth Cu parts without defects. Similar results were also obtained with scan speeds ranging from 450 to 500 mm/s and hatch distances from 0.08 to 0.09 mm (**Figure 3 (a)-(b**). Finally, scan speeds exceeding 500 mm/s yield rough and porous samples for the majority of the hatch distances investigated (**Figure 3 (a)-(b)**). The defects develop when insufficient laser energy is applied to the powder bed come from partial melting and sintering of the powders and subsequently result in pore generation [24]. XRD was performed on the as-received Cu powders and the printed parts for crystalline and phase evaluation in **Figure S1**. The diffractions peak at 2θ = 36, 43, 50 and 74 º are attributed to (-111), (111), (200) and (220) planes of the face-centered Cu [25]. No other peaks were observed other than Cu peaks in either the as-received Cu powders or the printed Cu parts. Additionally, the EDX analysis of the Cu powder and the printed parts can be found in **Figure S2**. The results show the presence of 7.7 and 2.4 wt.% of oxygen on the Cu

powder and printed parts respectively. Note that, the EDX measurement represents an estimation of the oxygen content in the feedstock and the printed part, and thus, cannot be interpreted as a quantitative analysis due to the measurement incertitude. The XRD and EDX analyses indicate that oxidation of Cu did not occur during the 3D printing step.

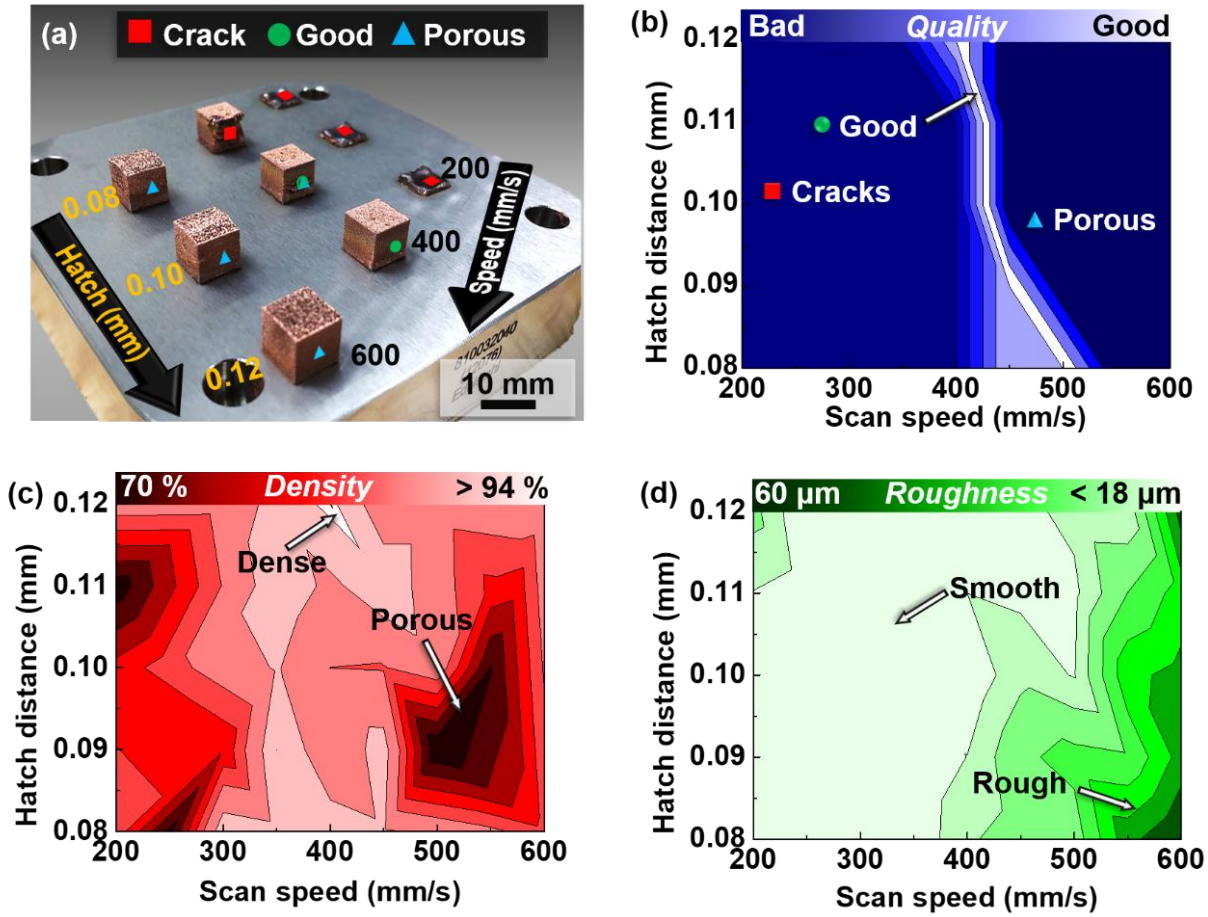

Figure 3. (a) Photo of printed Cu cubes with laser scan speeds from 200 – 600 m/s and hatch distances from 0.08 to 0.12 mm, respectively. **(b)** 2D map of the printing quality with respect to the scan speed and the hatch distance, **(c)** 2D map of the part density, and **(d)** the average surface roughness as a function of the scan speed and the hatch distance.

Part density and surface finish are the essential attributes to evaluate when assessing the print quality and optimizing process parameters. The densities of the printed Cu parts are summarized

in the 2D map as a function of the scan speed and the hatch distance in **Figure 3 (c)**. High-density parts were obtained within an extremely narrow processing window with a scanning speed of 400 mm/s and a hatch distance of 0.12 mm. A slight deviation in the scan speed or hatch distance from the optimized processing window significantly decreased the density of the printed part from ~95% to 70%. The average surface roughness (R_a) of the parts was measured using an optical profiler, with the results plotted in **Figure 3 (d)**. Using fast scan speeds (450 to 600 mm/s) for all hatch distances resulted in a large R_a (> 30 μm). Lower scan speeds led to a smaller R_a (< 18 μm). The R_a results at low and high scan speeds confirm the previous observations on part quality (**Figure 3(a)**). When the scan speed decreased, sufficient melting of the Cu powders occurred, leading to an adequate flow of molten metal, and thus, a low R_a [26]. The findings obtained by studying the part shape, density, and surface roughness, suggest that at a laser power of 400 W, a scan speed of 400 mm/s and a hatch distance of 0.12 mm are the optimal parameters to print a crack-free Cu part with a density of 95% and a R_a of 18 μm.

To better understand how the printing parameters, influence the density and R_a, the surface morphology of the printed parts was studied and associated with the molten metal stability. The laser-matter interactions induced the formation of a circular molten pool in several hundred microseconds[27]. Printing parameters, such as the scan speed and hatch distance, influence the dynamic, temperature, shape, and stability of the molten pool as well as the surface finish and the part density [17,28,29]. At a slow laser scanning speed of 200 mm/s, bumps form on the surface resulting in pores formation (**Figure 4 (a)** and **(b)**). The slow laser scanning speed generates a significant temperature gradient in the molten pool and induces a great difference in the surface tension between the edge and the center of the molten pool. As a result, the molten Cu tends to flow from the hot molten pool towards the colder edges of the pool, thus creating bumps at the

pool borders (**Figure 4 (b))** [30]. At 400 mm/s, the part shows a smooth and flat surface finish with minimal defects (**Figure 4 (c)** and **(e)**). At a moderate scan speed, the temperature of molten Cu is sufficiently high to achieve a desirable metal viscosity, resulting in a flat and stable molten pool, as illustrated in **Figure 4 (d)**. At 600 mm/s, the surface appears to be porous with balling effect (**Figure 4 (e)** and **(h)**). The insufficient laser energy deposition at a fast scan speed leads to an unstable molten pool (i.e., fluctuation), with poorly melted powders and a slow molten metal flow, leading to the formation of large pores (> 80 μm) (**Figure 4 (h)** and **(f)**) and bumps on the surface (i.e., the balling effect)[31].

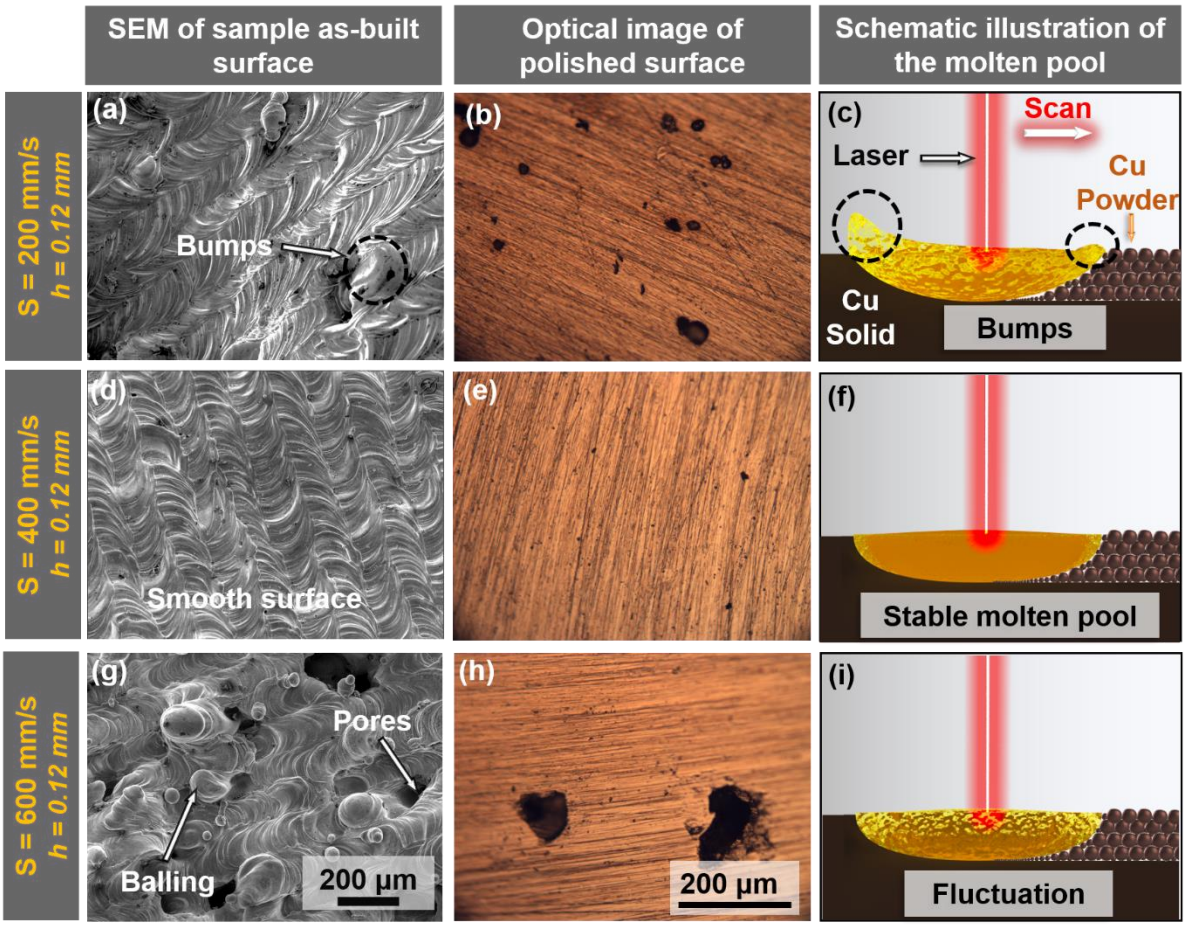

Figure 4. (a), (d), and **(g)** SEM micrographs of as-built surface sand **(b), (e),** and **(h)** optical images of polished surfaces with scan speeds of 200, 400, and 600 mm/s, respectively, and **(c), (f),** and **(i)** schematic illustrations of the molten pool shapes at different laser scan speeds.

Producing high-density Cu parts with moderate laser power is a critical advancement in additive manufacturing. Moderate power prevents damage to the laser optics (the back reflection of the laser beam) and lowers the energy consumption (60% less power compared to 1 KW laser) [32,33]. One possible explanation of the successful additive manufacturing of dense Cu parts with a moderate power is associated with the laser beam. Jadlhav *et al.* reported that low laser power led to porous Cu parts (84%) [12]. Others reported that adding oxide or carbon particles to the Cu parts enhanced the laser absorption, which should have decreased the laser power. Yet, high laser power was still required (> 500 W) [8,34]. Several studies demonstrated that the wavelength, beam angle, size, and quality play vital roles in laser-matter interactions [35–37]. Naturally, the laser beam characteristics influence the power required to manufacture Cu. The beam shape, size, and quality of the SLM 125 used in this study are presented in **Figure S3**. The beam quality (M^2) of the SLM 125 laser is 1.160, implying an excellent beam quality when focused on a small spot (*i.e.,* 70 μm) with the conservation of the original output power (*i.e.,* 400 W)[38,39].

The main advantage of the SLM is its ability to manufacture complex shapes that cannot be achieved by conventional machining techniques. The ability to design thin and sophisticated structures has the potential to significantly enhance the functionality of current heat sinks to cool electronic devices. The full potential of the SLM method was investigated by fabricating different heat sink structures, as presented in **Figure 5.** The first heat sink is a commercial (COM) columnar type. **Figure 5 (a)** and **(b)** show a photo and SEM micrographs of COM and

printed heat sinks having the same morphology and appearance with a column height of 12 mm and a diameter of 1.2 mm, respectively. The second type of heat sinks is a helix structure with a height and diameter of 12 mm and 750 μm, respectively (**Figure 5 (c)**). The third type of heat sinks consists of hallow, bent tubes with a pore diameter of 1 mm and a wall thickness of 300 μm, as shown in **Figure 5 (d)**. The optimal printing parameters (scan = 400 mm/s, hatch = 0.12 mm) were applied for the fabrication of complex structures with smooth, crack-free surfaces. It is worth mentioning that the printing of pure Cu shows a spatial resolution of a few hundred micrometers, which makes the SLM methods a desirable choice for the fabrication of complex thermal management components.

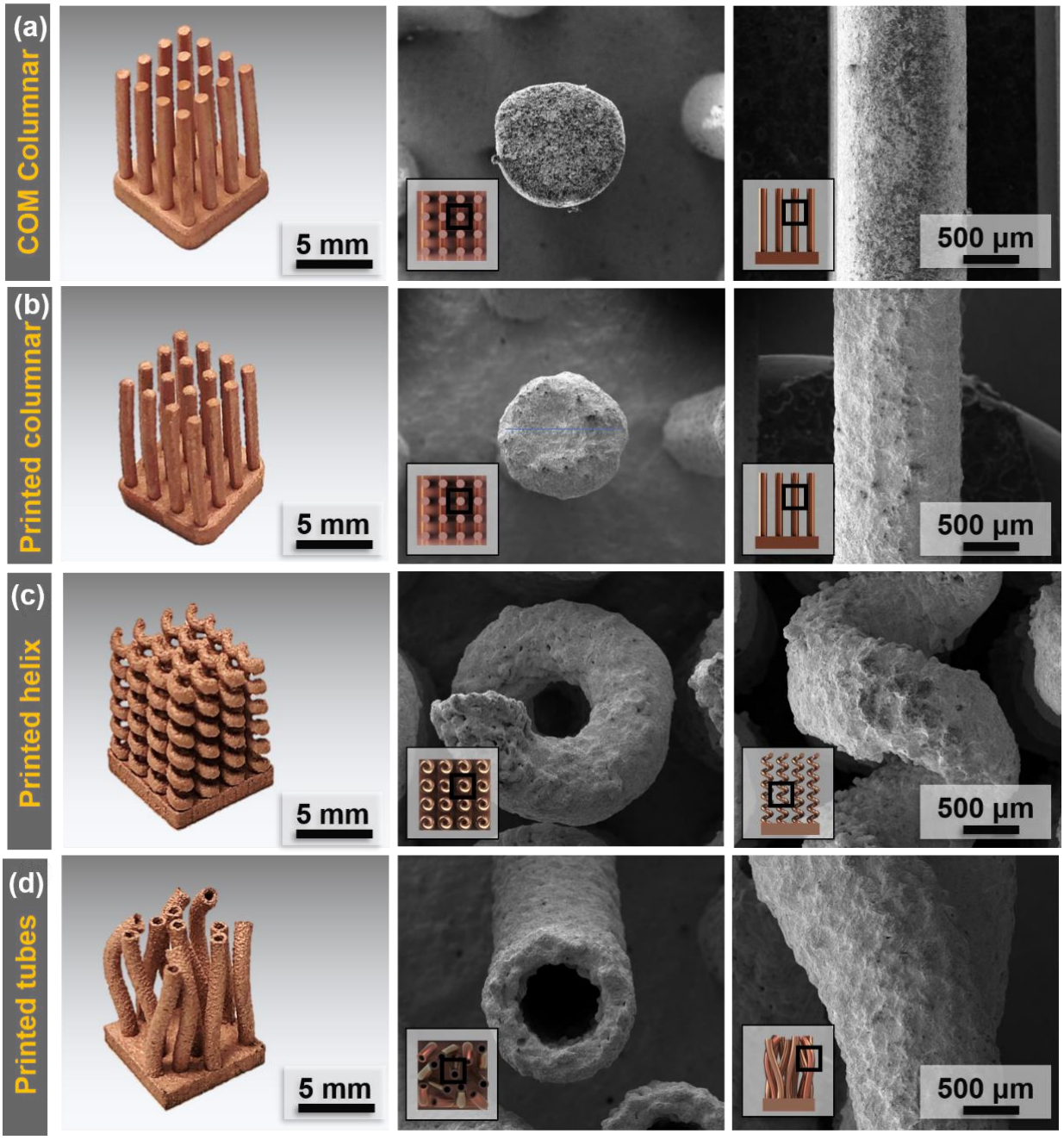

Figure 5. Top- and side-view photos and SEM micrographs of **(a)** a commercial (COM) columnar, **(b)** a printed columnar, **(c)** a printed helix, and **(d)** a printed bent tubes heat sink.

The physical properties of the columnar heat sink printed were measured and compared with the COM columnar heat sink and bulk Cu, as listed in **Table 1** [40–42]. Prior to the measurements, the printed and COM heat sinks were sandblasted to obtain a similar surface finish. The densities

of the printed and COM heat sinks were 95% and 98%, respectively. Note that the other structures also had densities of approximately 95% (*i.e.,* helix and bent tubes). The sample preparation and the current/voltage curve can be found in **Figure S4**. The resistance of a single Cu pillar was obtained by linear regression of the I/V curve and converted into electrical conductivity using the following equation [43]:

$$\sigma = \frac{L}{A \times R} \tag{2}$$

where σ is the electrical conductivity (S/m), L is the length of the pillar (m), A is the area cross-section (m^2), and R is the resistance (Ω). The results show that the printed and COM heat sinks have an electrical conductivity of 5.71 $\times 10^7$ and 5.81 $\times$ 10^7 S/m corresponding to 98 % IACS (International Annealed Copper Standard) and 100 % IACS, respectively (**Table 1**). Note that the incertitude in the electrical conductivity measurements is derived from the incertitude on the pillar dimensions measurement and the resistivity analysis. The electrical conductivity of the heat sinks appears elevated, considering their oxygen content and density. One explanation is that the small dimensions of the samples, imposed by COM heat sink (*i.e.,* length = 12 mm, diameter = 1.2 mm), may have inflated the electrical conductivity measurements. Therefore, one can still conclude that the printed and COM heat sinks possess comparable electrical properties.

The thermal conductivity can be obtained from the electrical conductivity measurement for pure metal using the Wiedemann-Franz law [44]:

$$\frac{\kappa}{\sigma} = KL \tag{3}$$

where κ is the thermal conductivity (W/m.K), K is the temperature (K), and L is a proportionality constant (2.2 x 10^{-8} $W\Omega/K^2$). The thermal conductivity of the printed and COM heat sinks was 368 and 378 W/m.K, respectively. The thermal conductivities of the commercial and printed heat

sinks measured in this study are comparable to the one measured by C. Vincent *et al.* on pure Cu prepared by a powder metallurgic route with similar density [41] as shown in Table 1.

Table 1. Physical properties of the printed and the commercial (COM) columnar heat sinks and bulk Cu

Properties	Printed heat sink	COM heat sink	Bulk Cu [40-42]
Density (%)	95	98	100
Electrical conductivity (S/m)	5.71 ± *0.26* x 10^7	5.81 ± *0.17* x 10^7	5.97 x 10^7
IACS (%)	98 ± *4*	100 ± *3*	103
Thermal conductivity (W/m.K)	368 ± *17*	378 ± *15*	385
Hardness (MPa)	108 ± *4*	72 ± *2*	60 - 120

The hardness of the printed and COM heat sinks was tested on the base plate. SEM micrographs of the indentation are presented in **Figure S5 (a)**. The hardness of the printed heat sink was found to be 108 MPa, which is higher than the COM one (72 MPa). The porosity and microstructure (*i.e.*, grain size) of the material affect the thermal and mechanical properties. Several studies demonstrated that the porosity mainly affects the thermal conductivity, while the microstructure alters the mechanical properties [41,45–47]. The grain size of the COM and printed heat sinks was measured, after acid etching, and presented in **Figure S5 (b)**. It was found that the grain size of the printed and COM samples was about 22 and 30 μm, respectively. A smaller microstructure hardened the material, producing better mechanical properties. Therefore, the printed heat sink possesses thermal properties similar to the COM one made out of pure Cu while being harder. The high thermal conductivity of the printed heat sink (i.e., 368 W/m.K) is

encouraging. We will explore the heat dissipation of SLM-printed heat sinks that can outperform the COM model.

The surface area is the main factor in thermal management. SLM has the ability to easily increase the specific surface area through manufacturing thin features of complex shapes [2,9]. To demonstrate the benefit of additive manufacturing in thermal management, the heat dissipation performance of different printed structures was measured and compared to a COM heat sink. **Figure 6 (a)** shows the experimental set-up where the heat sink was attached to a memory card chip placed on a hot plate heated to 100, 150, and 200 ºC, respectively. A fan was located 10 cm from the top of the heat sink to produce airflow. The temperature of the electronic chip was measured using an IR camera about 0.5 m from the heat sink. **Figure 6 (b)** displays the IR images of the heat sinks at 200 ºC. IR images for each structure and the chip temperature *vs.* time can be found in **Figure S6** and **S7**. The temperature of the chip alone was measured and subtracted from the chip temperature with different heat sink structures (cooling effect). **Figure 6 (c)** shows the cooling effect as a function of the heating temperature. The structures show similar cooling effects (-18 ºC) at 100 ºC. However, at 150 ºC, the structures begin to show different cooling effects, which become more pronounced when the heating temperature increases to 200 ºC. The printed and COM columnar structures have a similar cooling effect at about -36 ºC at 200 ºC. However, the helix and bent tubes heat sinks outperformed both types of columnar structures by reducing the chip temperature by -44 and -55 ºC, respectively. The superior cooling effect of the printed heat sinks is attributed to their increased surface area. As shown in **Figure 6 (d),** the bent tubes heat sink has the highest surface area of 600 mm^2/g, followed by the helix one with 390 mm^2/g, and the columnar heat sinks with 286 mm^2/g. In conclusion, using SLM to manufacture intricately shaped heat sinks yielded dense and crack-free parts with large surface

areas and excellent thermal properties. High dissipation performance is achieved with the SLM method and can produce heat-dissipating materials that exceed commercial ones.

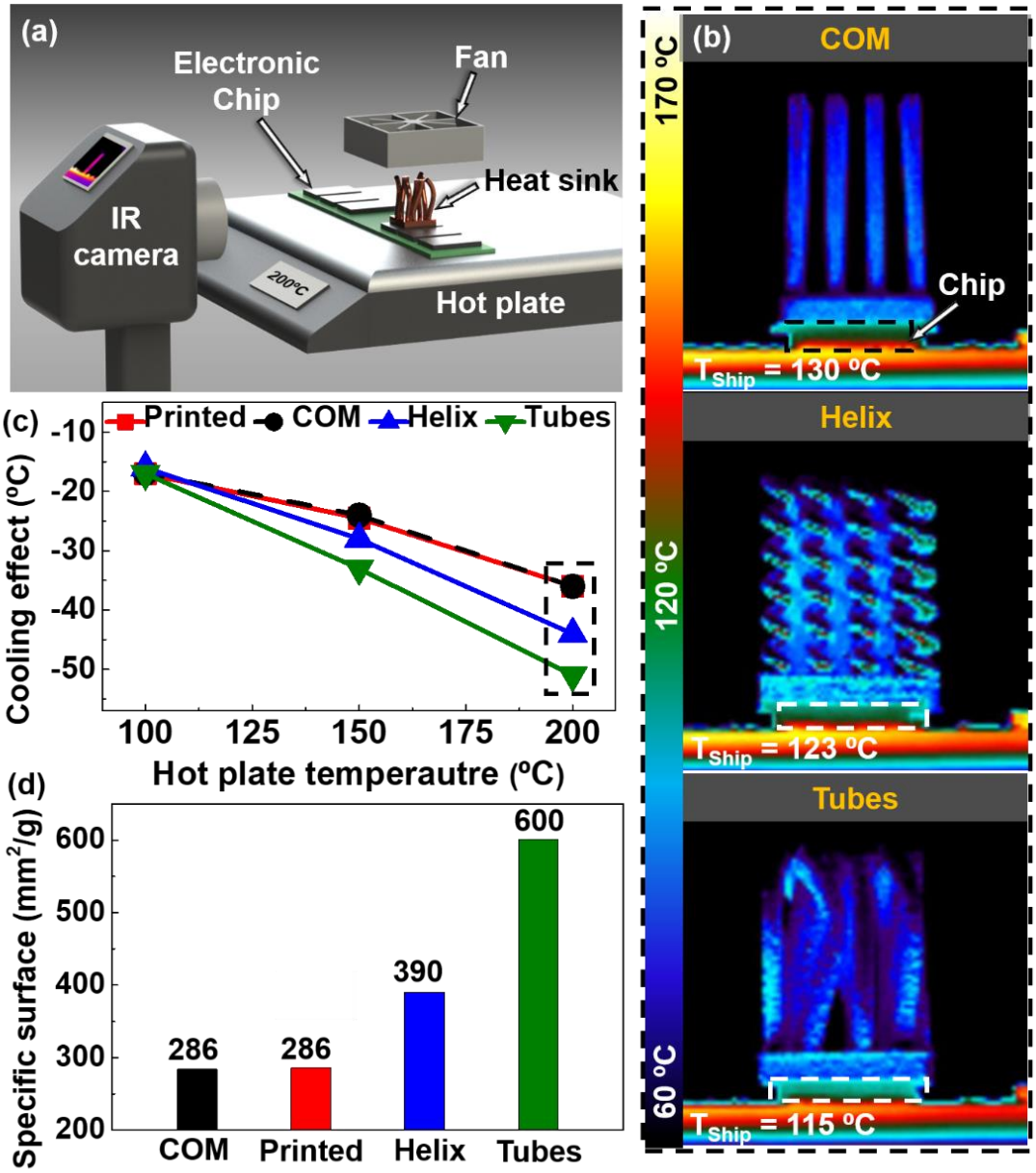

Figure 6. (a) Schematic illustration of the experimental set-up to measure the heat dissipation, **(b)** IR images of commercial (COM), helix and bent tubes heat sinks heated at 200 ºC, **(c)** Cooling effect (Cooling = $T_{chip} - T_{chip\ with\ heat\ sink}$) of different heat sinks as a function of heating temperature and **(d)** Specific surface area of heat sinks.

CONCLUSION:

In this study, SLM with a moderate laser power (400 W) was successfully implemented to additively manufacturing complex-shaped crack-free functional Cu parts that have a density up to 95% and a surface roughness of 18 μm. A systematic printing parameter development was performed to optimize the printing quality and understand the part formation mechanism. It was found that printing parameters play critical roles in controlling the printing quality. Insufficient energy deposition led to rough surface finish associated with bumps and pores, while excess energy deposition led to destructive balling effects, which could quickly fail the print. The high-density achieved in this study is attributed to a high-quality laser beam, which allows for uniform, focusing with the conservation of the original output power.

Functional Cu heat sinks with various sophistic structural designs were fabricated using the optimized printing parameter and their physical properties and thermal performance in cooling electronic chips were investigated. These printed Cu parts exhibited a thermal conductivity of 368 W/m.K, which is close to the bulk Cu fabricated using a powder metallurgy process (385 W/m.k).

The thermal performance of the printed Cu heat sinks was compared with commercially available Cu product by studying their cooling dissipation efficiency of a hot electronic chip. The COM and the printed columnar heat sinks with the same dimension showed similar cooling performances. However, the printed heat sinks with a helix structure and a unique thin and sophistic structure with bent porous tubes outperformed the COM columnar structure attributed to a significantly enhanced surface area. The development in additively manufacturing pure Cu parts will substantially improve the performance of the-state-of-art thermal components and

significant benefit the advancement of thermal management in a wide-range of fields, such as microelectronics, industrial heat sinks or military high-power high-frequency radar.

AUTHOR INFORMATION

Corresponding Authors

* Yong Feng Lu: ylu2@unl.edu; Jean-Francois Silvain: jean-francois.silvain@icmcb.cnrs.fr; Lisha Fan: s-lfan4@unl.edu

Author Contributions

‡ Loic Constantin and Zhipeng Wu contributed equally to this work. All authors approved the final version.

Acknowledgment

The authors are gratefully for the financial support provided by the National Science Foundation (CMMI 1826392) and the Nebraska Center for Energy Sciences Research (NCESR). The authors would like to thank Jamie Eske for her help on the English editing.

REFERENCES :

[1] L.L. Vasiliev, Heat pipes in modern heat exchangers, Applied Thermal Engineering. 25 (2005) 1–19. https://doi.org/10.1016/j.applthermaleng.2003.12.004.

[2] F. Singer, D.C. Deisenroth, D.M. Hymas, M.M. Ohadi, Additively manufactured copper components and composite structures for thermal management applications, in: 2017 16th IEEE Intersociety Conference on Thermal and Thermomechanical Phenomena in Electronic Systems (ITherm), 2017: pp. 174–183. https://doi.org/10.1109/ITHERM.2017.7992469.

[3] C. Körner, Additive manufacturing of metallic components by selective electron beam melting — a review, International Materials Reviews. 61 (2016) 361–377. https://doi.org/10.1080/09506608.2016.1176289.

[4] J. Lee, I. Mudawar, Two-phase flow in high-heat-flux micro-channel heat sink for refrigeration cooling applications: Part I—pressure drop characteristics, International

Journal of Heat and Mass Transfer. 48 (2005) 928–940. https://doi.org/10.1016/j.ijheatmasstransfer.2004.09.018.

[5] J.-F. Silvain, J.-M. Heintz, A. Veillere, L. Constantin, Y. Lu, A review of processing of Cu/C base plate composites for interfacial control and improved properties, Int. J. Extrem. Manuf. (2019). https://doi.org/10.1088/2631-7990/ab61c5.

[6] H. Zhang, L. Chen, Y. Liu, Y. Li, Experimental study on heat transfer performance of lotus-type porous copper heat sink, International Journal of Heat and Mass Transfer. 56 (2013) 172–180. https://doi.org/10.1016/j.ijheatmasstransfer.2012.08.047.

[7] W.E. Frazier, Metal Additive Manufacturing: A Review, J. of Materi Eng and Perform. 23 (2014) 1917–1928. https://doi.org/10.1007/s11665-014-0958-z.

[8] S.D. Jadhav, S. Dadbakhsh, J. Vleugels, J. Hofkens, P. Van Puyvelde, S. Yang, J.-P. Kruth, J. Van Humbeeck, K. Vanmeensel, Influence of Carbon Nanoparticle Addition (and Impurities) on Selective Laser Melting of Pure Copper, Materials. 12 (2019) 2469. https://doi.org/10.3390/ma12152469.

[9] R. Neugebauer, B. Müller, M. Gebauer, T. Töppel, Additive manufacturing boosts efficiency of heat transfer components, Assembly Automation. (2011). https://doi.org/10.1108/01445151111172925.

[10] D.A. Ramirez, L.E. Murr, S.J. Li, Y.X. Tian, E. Martinez, J.L. Martinez, B.I. Machado, S.M. Gaytan, F. Medina, R.B. Wicker, Open-cellular copper structures fabricated by additive manufacturing using electron beam melting, Materials Science and Engineering: A. 528 (2011) 5379–5386. https://doi.org/10.1016/j.msea.2011.03.053.

[11] T.Q. Tran, A. Chinnappan, J.K.Y. Lee, N.H. Loc, L.T. Tran, G. Wang, V.V. Kumar, W. a. D.M. Jayathilaka, D. Ji, M. Doddamani, S. Ramakrishna, 3D Printing of Highly Pure Copper, Metals. 9 (2019) 756. https://doi.org/10.3390/met9070756.

[12] S.D. Jadhav, S. Dadbakhsh, L. Goossens, J.-P. Kruth, J. Van Humbeeck, K. Vanmeensel, Influence of selective laser melting process parameters on texture evolution in pure copper, Journal of Materials Processing Technology. 270 (2019) 47–58. https://doi.org/10.1016/j.jmatprotec.2019.02.022.

[13] C. Silbernagel, L. Gargalis, I. Ashcroft, R. Hague, M. Galea, P. Dickens, Electrical resistivity of pure copper processed by medium-powered laser powder bed fusion additive manufacturing for use in electromagnetic applications, Additive Manufacturing. 29 (2019) 100831. https://doi.org/10.1016/j.addma.2019.100831.

[14] A. Hess, R. Schuster, A. Heider, R. Weber, T. Graf, Continuous Wave Laser Welding of Copper with Combined Beams at Wavelengths of 1030nm and of 515nm, Physics Procedia. 12 (2011) 88–94. https://doi.org/10.1016/j.phpro.2011.03.012.

[15] L. Constantin, L. Fan, B. Mortaigne, K. Keramatnejad, Q. Zou, C. Azina, Y.F. Lu, J.-F. Silvain, Laser sintering of cold-pressed Cu powder without binder use, Materialia. 3 (2018) 178–181. https://doi.org/10.1016/j.mtla.2018.08.021.

[16] M. Colopi, L. Caprio, A.G. Demir, B. Previtali, Selective laser melting of pure Cu with a 1 kW single mode fiber laser, Procedia CIRP. 74 (2018) 59–63. https://doi.org/10.1016/j.procir.2018.08.030.

[17] T.-T. Ikeshoji, K. Nakamura, M. Yonehara, K. Imai, H. Kyogoku, Selective Laser Melting of Pure Copper, JOM. 70 (2018) 396–400. https://doi.org/10.1007/s11837-017-2695-x.

[18] S. Zhang, H. Zhu, L. Zhang, W. Zhang, H. Yang, X. Zeng, Microstructure and properties of high strength and high conductivity Cu-Cr alloy components fabricated by high power selective laser melting, Materials Letters. 237 (2019) 306–309. https://doi.org/10.1016/j.matlet.2018.11.118.

[19] S. Zhang, H. Zhu, Z. Hu, X. Zeng, F. Zhong, Selective Laser Melting of Cu10Zn alloy powder using high laser power, Powder Technology. 342 (2019) 613–620. https://doi.org/10.1016/j.powtec.2018.10.002.

[20] M. Sabelle, M. Walczak, J. Ramos-Grez, Scanning pattern angle effect on the resulting properties of selective laser sintered monolayers of Cu-Sn-Ni powder, Optics and Lasers in Engineering. 100 (2018) 1–8. https://doi.org/10.1016/j.optlaseng.2017.06.028.

[21] E.O. Olakanmi, R.F. Cochrane, K.W. Dalgarno, A review on selective laser sintering/melting (SLS/SLM) of aluminium alloy powders: Processing, microstructure, and properties, Progress in Materials Science. 74 (2015) 401–477. https://doi.org/10.1016/j.pmatsci.2015.03.002.

[22] J.-P. Kruth, G. Levy, F. Klocke, T.H.C. Childs, Consolidation phenomena in laser and powder-bed based layered manufacturing, CIRP Annals. 56 (2007) 730–759. https://doi.org/10.1016/j.cirp.2007.10.004.

[23] M.F. Zaeh, G. Branner, Investigations on residual stresses and deformations in selective laser melting, Prod. Eng. Res. Devel. 4 (2010) 35–45. https://doi.org/10.1007/s11740-009-0192-y.

[24] Y. Mingchuan, S. Zhenzhen, L.U. Ke, Y. Mingchuan, S. Zhenzhen, L.U. Ke, Synthesis of W--20%Cu Nanocomposite Powders, Acta Metall. 40 (2004) 639. http://www.ams.org.cn/EN/abstract/abstract3857.shtml (accessed September 13, 2019).

[25] M. Raffi, S. Mehrwan, T.M. Bhatti, J.I. Akhter, A. Hameed, W. Yawar, M.M. ul Hasan, Investigations into the antibacterial behavior of copper nanoparticles against Escherichia coli, Ann Microbiol. 60 (2010) 75–80. https://doi.org/10.1007/s13213-010-0015-6.

[26] A.H. Maamoun, Y.F. Xue, M.A. Elbestawi, S.C. Veldhuis, Effect of Selective Laser Melting Process Parameters on the Quality of Al Alloy Parts: Powder Characterization, Density, Surface Roughness, and Dimensional Accuracy, Materials (Basel). 11 (2018). https://doi.org/10.3390/ma11122343.

[27] A.V. Gusarov, I. Yadroitsev, P. Bertrand, I. Smurov, Model of Radiation and Heat Transfer in Laser-Powder Interaction Zone at Selective Laser Melting, J. Heat Transfer. 131 (2009). https://doi.org/10.1115/1.3109245.

[28] D. Dai, D. Gu, Tailoring surface quality through mass and momentum transfer modeling using a volume of fluid method in selective laser melting of TiC/AlSi10Mg powder, International Journal of Machine Tools and Manufacture. 88 (2015) 95–107. https://doi.org/10.1016/j.ijmachtools.2014.09.010.

[29] J. Yin, L. Yang, X. Yang, H. Zhu, D. Wang, L. Ke, Z. Wang, G. Wang, X. Zeng, High-power laser-matter interaction during laser powder bed fusion, Additive Manufacturing. 29 (2019) 100778. https://doi.org/10.1016/j.addma.2019.100778.

[30] B. Xiao, Y. Zhang, Marangoni and Buoyancy Effects on Direct Metal Laser Sintering with a Moving Laser Beam, Numerical Heat Transfer, Part A: Applications. 51 (2007) 715–733. https://doi.org/10.1080/10407780600968593.

[31] L. Wang, S. Wang, J. Wu, Experimental investigation on densification behavior and surface roughness of AlSi10Mg powders produced by selective laser melting, Optics & Laser Technology. 96 (2017) 88–96. https://doi.org/10.1016/j.optlastec.2017.05.006.

[32] Ytterbium Multi-mode CW Lasers, Up to 2.5 kW | IPG Photonics, (n.d.). https://www.ipgphotonics.com/en/products/lasers/mid-power-cw-fiber-lasers/1-micron/ylm-mm-and-ylr-mm#[ylm-mm-200-400-w] (accessed September 30, 2019).

[33] Ytterbium Multi-mode CW Lasers, Up to 2.5 kW | IPG Photonics, (n.d.). https://www.ipgphotonics.com/en/products/lasers/mid-power-cw-fiber-lasers/1-micron/ylm-mm-and-ylr-mm#[ylr-mm-wc-1000-2000-w] (accessed September 30, 2019).

[34] S.D. Jadhav, J. Vleugels, J.-P. Kruth, J.V. Humbeeck, K. Vanmeensel, Mechanical and electrical properties of selective laser-melted parts produced from surface-oxidized copper powder, Material Design & Processing Communications. 0 (n.d.) e94. https://doi.org/10.1002/mdp2.94.

[35] M.S. Brown, C.B. Arnold, Fundamentals of Laser-Material Interaction and Application to Multiscale Surface Modification, in: K. Sugioka, M. Meunier, A. Piqué (Eds.), Laser Precision Microfabrication, Springer Berlin Heidelberg, Berlin, Heidelberg, 2010: pp. 91–120. https://doi.org/10.1007/978-3-642-10523-4_4.

[36] G.E. Bean, D.B. Witkin, T.D. McLouth, D.N. Patel, R.J. Zaldivar, Effect of laser focus shift on surface quality and density of Inconel 718 parts produced via selective laser melting, Additive Manufacturing. 22 (2018) 207–215. https://doi.org/10.1016/j.addma.2018.04.024.

[37] G.C. Rodrigues, V. Vorkov, J.R. Duflou, Optimal laser beam configurations for laser cutting of metal sheets, Procedia CIRP. 74 (2018) 714–718. https://doi.org/10.1016/j.procir.2018.08.026.

[38] A.E. Siegman, Defining, measuring, and optimizing laser beam quality, in: Laser Resonators and Coherent Optics: Modeling, Technology, and Applications, International Society for Optics and Photonics, 1993: pp. 2–12. https://doi.org/10.1117/12.150601.

[39] X. Luo, P. Chen, Y. Wang, Power content M2-values smaller than one, Appl. Phys. B. 98 (2009) 181. https://doi.org/10.1007/s00340-009-3623-8.

[40] R.A. Matula, Electrical resistivity of copper, gold, palladium, and silver, Journal of Physical and Chemical Reference Data. 8 (1979) 1147–1298. https://doi.org/10.1063/1.555614.

[41] C. Vincent, J.F. Silvain, J.M. Heintz, N. Chandra, Effect of porosity on the thermal conductivity of copper processed by powder metallurgy, Journal of Physics and Chemistry of Solids. 73 (2012) 499–504. https://doi.org/10.1016/j.jpcs.2011.11.033.

[42] J. Yu, G. Wang, Y. Rong, Experimental Study on the Surface Integrity and Chip Formation in the Micro Cutting Process, Procedia Manufacturing. 1 (2015) 655–662. https://doi.org/10.1016/j.promfg.2015.09.063.

[43] Y. Lu, L.M. Santino, S. Acharya, H. Anandarajah, J.M. D'Arcy, Studying Electrical Conductivity Using a 3D Printed Four-Point Probe Station, J. Chem. Educ. 94 (2017) 950–955. https://doi.org/10.1021/acs.jchemed.7b00119.

[44] Theoretical Solid State Physics, Courier Corporation, 1985.

[45] D.A. Ramirez, L.E. Murr, E. Martinez, D.H. Hernandez, J.L. Martinez, B.I. Machado, F. Medina, P. Frigola, R.B. Wicker, Novel precipitate–microstructural architecture developed in the fabrication of solid copper components by additive manufacturing using electron beam melting, Acta Materialia. 59 (2011) 4088–4099. https://doi.org/10.1016/j.actamat.2011.03.033.

[46] E. Botcharova, J. Freudenberger, L. Schultz, Mechanical and electrical properties of mechanically alloyed nanocrystalline Cu–Nb alloys, Acta Materialia. 54 (2006) 3333–3341. https://doi.org/10.1016/j.actamat.2006.03.021.

[47] O.V. Gendelman, M. Shapiro, Y. Estrin, R.J. Hellmig, S. Lekhtmakher, Grain size distribution and heat conductivity of copper processed by equal channel angular pressing, Materials Science and Engineering: A. 434 (2006) 88–94. https://doi.org/10.1016/j.msea.2006.06.091.